

The Velocity and Attenuation of Acoustic Emission Waves in SiC/SiC Composites Loaded in Tension

Gregory N. Morscher and Andrew L. Gyekenyesi
Ohio Aerospace Institute*; Cleveland, Ohio

ABSTRACT

The behavior of acoustic waves produced by microfracture events and from pencil lead breaks was studied for two different silicon carbide fiber-reinforced silicon carbide matrix composites. The two composite systems both consisted of Hi-Nicalon™ fibers and carbon interfaces but had different matrix compositions that led to considerable differences in damage accumulation and acoustic response. This behavior was primarily due to an order of magnitude difference in the interfacial shear stress for the two composite systems. Load/unload/reload tensile tests were performed and measurements were made over the entire stress range in order to determine the stress-dependence of acoustic activity for increasing damage states. It was found that using the extensional wave velocities from acoustic emission (AE) events or AE produced from pencil lead breaks performed outside of the transducers enabled accurate measurements of the stiffness of the composite. The extensional wave velocities changed as a function of the damage state and the stress where the measurement was taken. Attenuation for AE waveforms from the pencil lead breaks occurred only for the composite possessing the lower interfacial shear stress and only at significantly high stresses. At zero stress after unloading from a peak stress, no attenuation occurred for this composite because of crack closure. For the high interfacial stress composite no attenuation was discernable at peak or zero stress over the entire stress-range of the composite. From these observations, it is believed that attenuation of AE waveforms is dependent on the magnitude of matrix crack opening.

Keywords: *Ceramic matrix composites (CMCs), Matrix cracking, Acoustic emission*

INTRODUCTION

A desirable attribute of ceramic matrix composites (CMCs) is their non-linear stress-strain behavior when loaded in tension [1] and sometimes referred to as “graceful failure”. This attribute combined with high-temperature durability makes CMCs potential materials for applications such as combustor liners of future high-performance civil aircraft engines [2]. The nonlinear response is mostly the result of transverse matrix cracks, although, additional damage mechanisms such as interlaminar matrix cracks (i.e., interlaminar delaminations) and fiber breaks may also contribute to this behavior. The underlying feature that governs the energy absorbing process of damage accumulation in CMCs is the interface that lies between the fibers and the

1 This report is a preprint of an article submitted to a journal for publication. Because of changes that may be made before formal publication, this preprint is made available with the understanding that it will not be cited or reproduced without the permission of the author.

matrix. A properly planned interface allows matrix cracks to propagate around fibers, via the interface, rather than fracturing the fiber itself. This results in matrix cracks that are bridged by unbroken fibers. In the vicinity of the matrix cracks, the bridging fibers experience higher strains than fibers in areas without matrix cracks, which is the cause of the non-linearity. The extent of non-linearity is predominantly due to the interfacial shear strength, i.e. lower interfacial shear strengths result in longer load-transfer lengths between fiber and matrix, wider crack-openings at stress, and therefore larger non-linear strains at a given stress in comparison to a similar composite with a higher interfacial shear stress.

Acoustic waves, i.e. acoustic emission (AE), are created when matrix cracks are formed, propagated, or opened. AE has been used to monitor or measure the degree of damage in ceramic matrix composites. For example, AE has proven to be an excellent technique for determining when the first matrix cracks appear [3]. It should be noted that the first damage events usually occur at stress levels prior to the initiation of non-linear behavior. AE has also proven successful in monitoring the accumulation of damage during tensile tests [4-6] as well as correlating the individual AE signals to specific damage events [7-8].

With the formation of matrix cracks, the stiffness of the composite decreases. Consequently, the transmission of acoustic waves changes in the form of slower velocities and increased attenuation. The acoustic activity in the composite specimens are all considered to be plate waves since the wavelengths are on the order of 1 to 2 cm and the smallest dimension of the tensile bars, i.e. thickness, are approximately 2 mm [9]. There are essentially two modes ^{at that or} _{which} sound wave travel in plates over long distances: the extensional/longitudinal wave (akin to the pressure wave in bulk material) and the flexural/shear wave [10]. The extensional wave is always faster than the flexural wave and the speed of the extensional wave is practically independent of the frequency of the wave itself, i.e., non-dispersive [7]. The speed of acoustic waves will be slower with the accumulation of damage in a composite since the stiffness of the specimen decreases with increasing damage. In reference 7 the speed of the extensional component of an acoustic emission waveform decreased with increasing damage to the same degree that the square root of the elastic modulus decreased, in accordance with plate wave theory [9]. In addition, it has been shown that acoustic waves introduced via a transducer, as in

* Resident Senior Research Scientists at NASA Glenn Research Center, Cleveland, Ohio

the case of acousto-ultrasonics (AU), attenuate relative to the amount of damage accumulation in the material [11].

In this study, the effect of damage accumulation on both the speed of sound and attenuation of acoustic emission waves at different stresses and damage states was evaluated. Load-unload-reload tensile hysteresis tests were performed on materials that were similar to the well studied SiC(fiber)/SiC(matrix) composite system evaluated by Morscher [7]. The AE caused by microfracture and sliding events in the composite specimen was monitored during tensile testing and for the most part only occurs at loads beyond the prior maximum load used in the previous unload-reload cycle, i.e. the "Kaiser effect" [12]. In addition, at various load increments during unloading and reloading, the load was held constant and pencil lead breaks were performed outside of the AE sensors to measure the speed of sound as well as loss or damping in the signal as a function of stress. In this way, the influence of the stress state of the material was analyzed by varying the static stress state of the material while maintaining a constant state of damage below the peak stress of the hysteresis loop.

EXPERIMENTAL

Room temperature load/unload/reload tensile tests were performed on Hi-NicalonTM (Nippon Carbon, Japan) reinforced chemical vapor infiltrated (CVI) SiC matrix composites^{**}. All the composites were composed of eight plies of balanced, 8-harness satin woven fiber cloth. The woven cloth was stacked in a 0/90 fashion. An interphase layer, approximately 0.5 μm in thickness, consisted of carbon that was applied by the chemical vapor infiltration (CVI) method. There were two CVI SiC matrices studied, one consisted of just CVI SiC (STD) and the second consisted of an enhanced matrix (ENH) that included boron carbide (B_4C) additions. The two composites tested in this study are listed in Table I along with relevant constituent and composite properties.

AE was monitored with a Fracture Wave Detector (FWD)[#] system utilizing wide band (50 to 2000 khz) sensors (Model B1025[#]). The system is relatively unique in the fact that it digitizes the true, multiple-frequency waveform (modal AE) rather than just calculating certain parameters of the waveform based on a single-frequency damped sine curve. The FWD system

^{**} Manufactured by Honeywell Composites,
[#] Digital Wave Corporation, Englewood CO

consisted of a Pentium 120 MHz based computer with an 8-bit, 30 MHz acquisition A/D board. Each sensor was connected to a preamplifier and filter trigger module that was fed into the computer. The preamplifier was set at 20 dB, the filter signal was amplified 9 dB and the filter trigger was amplified 21 dB. The load and strain were also recorded with the FWD computer via 10 volt signals provided by the hydraulic load frame. The post-test analysis was conducted using Wave Detector™ software provided by the FWD manufacturer.

The test procedure for each specimen was as follows. While the specimen was gripped in the load frame, prior to applying the load, pencil lead breaks (0.5 mm HB) were performed on the specimen's face in a location outside of all the ultrasonic transducers (Figure 1). These lead breaks were conducted in order to obtain a velocity measurement for the extensional wave in the undamaged state [7]. The extensional waves travel faster than the flexural waves and thereby arrive first at the sensors. This allows for easy identification. The specimens were mechanically loaded in a repeated load-unload fashion. With each reload, the maximum stress level was progressively increased. For a typical experiment, the stress was increased to a stress level of 69 MPa and then unloaded to zero stress. This was followed by stress reversal points of 138 MPa, 207 MPa, 276 MPa, 345 MPa, and then finally to failure. The increasing stress rate was 0.69 MPa/second, while the decreasing stress rate was 2.1 MPa/second. The increasing stress rate was slow enough to allow the FWD system to capture most of the AE activity. For various reasons, slight deviations of the stress reversal points were selected so as to allow each specimen's experimentation to be tailored. For example, some tests were interrupted before failure to allow sectioning for microscopy. The load was held numerous times during the tests to allow for pencil lead breaks on the specimen face. The holds were conducted at specified stress levels both during the load-up to the peak stress as well as numerous times during the unload from the peak stress to zero stress. Note that by taking numerous measurements during the unload and reload portion of the tests, the stress dependence of certain acoustic parameters could be studied. This was due to the fact the stress was changing while the damage state was held constant. Again, these lead breaks were conducted outside of the transducers. This allowed velocity measurements, as well as attenuation readings, to be made as the wave traveled past each of the AE transducers.

RESULTS

Acoustic Emission Activity During Tensile Testing

The mechanical behavior and AE activity observed for the materials in this study were very similar to earlier studies concerning comparable materials [7,8]. Typical stress-strain plots from load-unload tensile tests are shown in Figure 2. As the extent of non-linearity increases, the width of the hysteresis loops also increase. Figure 2a and 2b indicate the AE activity, in the form of accumulated AE energy. AE energy was found to have a nearly direct relationship to the amount of transverse matrix cracking in these types of composites [7,8]. Therefore, most matrix crack formation and propagation occurred between 0.05 and 0.35 percent strain for all the composites. Matrix crack saturation, as evidenced by the drastic reduction in the rate of cumulative AE energy, occurred at $\sim 0.35\%$ (~ 200 MPa for the HN-C-STD composite and ~ 250 MPa for the HN-C-ENH composite). It should be noted that AE events occurring outside of the two AE transducers were discarded from the cumulative energy analysis (see reference 7).

The Use of Acoustic Emission Waveforms to Monitor Elastic Modulus

The AE data was used to measure the velocity of sound of the extensional component, $C_{e(\sigma)}$, of the AE waveforms. This was accomplished by utilizing actual fracture events that occurred outside of both the sensors. Next, the velocity was related to the elastic modulus of the specimen as a function of the load history, defined by the maximum stress attained during the particular hysteresis loop [7]. From the distance between the AE sensors, x , (Figure 1) and the difference in times of arrival of the first peak, Δt_x , as the waveforms pass each sensor (Figure 3), the experimentally determined velocity of the extensional wave can be calculated [7]:

$$C_{e(\sigma)} = x / \Delta t_x \quad (1)$$

The speed of sound was measured for the untested material, $C_{e(\sigma=0)}$, from AE created from the lead breaks performed outside of the sensors. Note again that σ in equation (1) defines the peak stress of a given hysteresis loop. Also, the AE events used for the velocity measurement in Figure 3 occurred at the peak stress achieved up to that point during the tensile test.

From classical plate theory [9,10] where the wavelength is much larger than the plate thickness and the direction of wave propagation is in the main symmetry direction of an orthotropic laminated plate, the velocity of an extensional wave, C_e , is related to the longitudinal elastic modulus, E , in the following form:

$$C_e = [E / \{ \rho h \}]^{1/2} \quad (2)$$

where ρ is the density of the material and h is the plate thickness (~ 2 mm). The elastic response for any particular hysteresis loop was defined by two methods. First, the initial tangent modulus at the beginning of a reloading cycle was used. Second, the unloading tangent modulus was obtained at the beginning of the unload after reaching the peak stress [13]. The loading and unloading portion of the hysteresis loop were fit with a polynomial equation. The instantaneous elastic modulus was then found from the derivative of the polynomial equation at the strains for initial loading and unloading of the hysteresis curves [13]. To compare the measured velocities with the measured elastic moduli, the normalized speed of sound ($C_{e(\sigma)} / C_{e(\sigma=0)}$) was compared to the square root of the normalized elastic modulus, $(E_{(\sigma)} / E_{(\sigma=0)})^{1/2}$, for each hysteresis loop, after equation (2). As described below, the speed of sound was measured from either microfracture events that occurred outside of the sensors or from pencil lead breaks that were performed outside of the sensors. Figure 3 shows a typical result for a HN-C-ENH composite. There was excellent agreement between the unload elastic modulus and the measured speed of sound. Similar results were also observed in reference 7.

In each case, the reloading elastic modulus was higher than the unloading elastic modulus. This was also observed for SiC/SiC composites in reference 13. Since the AE velocity data was obtained at stresses higher than the previous peak stress and never during unloading or reloading, i.e. at lower stresses than the peak stress, the measured velocity is expected to correspond to the unload elastic modulus.

The larger reloading elastic modulus at zero stress after matrix cracking is assumed to be due to matrix crack closure at a positive tensile stress. This is the result of residual compressive stresses in the matrix (e.g. due to thermal expansion mismatch between the fiber and the matrix) or to debris that may accumulate in the matrix cracks during cycling. A method has been defined which can approximate the existence of internal residual stresses in a composite [14]. It has been

shown that the location of the point of intersection of the average slopes of the hysteresis curves above the closure stress will define whether residual stresses are tensile, compressive or zero. If the point of intersection is at a positive stress, then the matrix residual stresses are compressive; if the point of intersection is at a negative stress, then the matrix residual stresses are tensile; and if the point of intersection is at zero stress then there are no residual stresses. For these composites the intersection is essentially zero stress or a negative stress as seen in Figure 2. Therefore, from this reasoning it appears that the cause for the crack closure effect is due to debris in the matrix crack.

Analysis of Pencil Lead Breaks using the AE System

Little if any AE emission occurred during the unloading portion of the hysteresis loops or during the reloading at stresses below the previous peak stress (Kaiser effect). Pencil lead breaks were performed during load-holds of the tensile tests in order to determine the extensional-wave velocity of sound across the two AE sensors as a function of stress during the unloading and reloading portion of the test. Figure 4 shows typical captured waveforms for each of the two AE sensors. In the figure, two lead breaks were conducted; one at the peak stress of 207 MPa (Figure 4a) and the other at zero stress after unloading from the peak stress (Figure 4b). It can be seen for each stress case that the amplitudes of the waveforms at the far sensor, as indicated by the later arrival time, were much lower. This shows that extensive damping occurred as the wave traveled through the material between the sensors. The issue of attenuation as measured using AE energy is discussed later in this section.

The velocity of the extensional waves as measured during each load hold for the HN-C-STD and HN-C-ENH composites are plotted in Figures 5a and 5b, respectively. The wave velocities are plotted as a function of time. Here, the time variable allows for representations of each of the velocity measurements made during the successive holds. As one moves from left to right on the plot, the velocity values are indicated for each hold during the loading as well as unloading stages. For clarity and for showing the relationship between stress and extensional wave velocity, the stress level at each particular time is also indicated in the plot. Note that in general there is a decreasing trend concerning the velocity of the extension wave. This indicates that with each load-unload curve the damage level is increased, and as a result the modulus of the

material is decreased as observed in Figure 3. Also evident in Figure 5 is a stress dependent velocity for the extensional wave. As the specimens were unloaded from the peak stresses, the velocity measurements show an increase. No further damage was induced during the unload. Even so, the tangent modulus continuously changes as the specimens were unloaded from the peak stress to zero stress (see Figure 2).

Figure 6 shows the $C_{e(\sigma)} / C_{e(\sigma=0)}$ from lead breaks and $(E_{(\sigma)}/E_{(\sigma=0)})^{1/2}$ from tangent moduli at both the peak stress as well as the zero stress for various values of peak hysteresis stress. There is excellent correlation between the velocity and tangent modulus values for both measurements made at the peak stress as well as measurements made at zero stress for both composite systems. This confirms that the velocity of sound waves mimics the elastic response (stiffness) of the system (equation 1) even when affected by a residual stress-state, e.g. crack-closure. It should be noted that the tangent modulus, at points other than at initial stress-up (loading) or stress-down (unloading), decreases with increasing stress upon further loading or decreasing stress upon further unloading. This is due to the shear-lag mechanism of fiber sliding and is the cause of the hysteresis loop. Therefore, the tangent modulus of the unloading or reloading curve other than the initial tangent modulus is not a true elastic response [15].

Attenuation of AE Waveforms

As stated above, some damping had occurred as the extensional wave traversed the material between the two AE sensors. This is evident in Figures 3 and 4 where the sensor that was closer to the material fracture source or lead break source had a larger maximum amplitude than the farther sensor. The maximum amplitude for these events is composed of the flexural wave, which is typical for plate waves.

In order to quantify the degree of signal loss between the two sensors, the loss in peak amplitudes and waveform energy were considered. Unfortunately, most of the recorded events saturated the amplitude scale, i.e. were greater than 1 mV, on the sensor nearest to the AE source. This made it impossible to accurately compare the amplitudes of the near and far sensors. The use of energy was complicated by the fact that only 82 μ s were recorded for each time event. This meant that the amount of the flexural wave (the major contributor to the energy of the waveform) captured on the far sensor was significantly less than on the near sensor.

Fortunately, the software can perform an operation* whereby only a portion of the waveform is analyzed. The portion is centered about a point in the time-domain where the waveform first reaches a predetermined threshold voltage. For this study, a threshold voltage of 200 mV and a time-domain of 25 μ s were used. This threshold voltage was lower than the peak of the first flexural wave but was sufficient to exceed the extensional wave peak amplitude. The time-domain of 25 μ s was less than the total time that the flexural wave was captured on the far sensor and made for a valid comparison between the near and far sensor (see Figure 4). The ratio of energy over that 25 μ s time frame was then compared by dividing the energy from the far sensor by the energy of the near sensor. This results in a fraction or ratio of energy that was transmitted across the specimen in between the two sensors. It should be noted that only the events that had less than two percent of the waveform saturated in the time domain were used for the energy analysis. This reduced the error due to amplitude saturation.

The energy ratio for an undamaged specimen was approximately 0.43 for both the HN-C-STD and HN-C-ENH composites (Figure 7). In other words, a little over half the signal energy is naturally lost over the distance between the two sensors. For the HN-C-STD composite, a significant drop in transmitted AE energy is observed between 138 and 207 MPa for the attenuation measurements made at the peak stress (Figure 7a). Note that only attenuation measurements made at the peak stress, where cracks are held open, showed the drastic changes. Changes in the attenuation were not observed when the measurements were made at zero stress after unloading from the peak stress (Figure 7a). However, for specimens stressed to peak stresses greater than 138 MPa (207 or 276 MPa), significant attenuation was observed when intermediate stresses greater or equal to 69 MPa were applied (Figure 8). For the HN-C-ENH no significant changes in attenuation were observed with increasing peak stress or for measurements made at zero stress after unloading from the peak stress (Figure 7b). It is speculated that the attenuation behavior observed for the two different composites measured at the two different stress-states is dependent on the degree of crack opening as will be discussed below.

* TCOT™ is a time-centered on threshold voltage analysis performed by the Wave Detector post test software provided with the Digital Wave Fracture Wave Detector.

Crack Density and Interfacial Shear Strength Analysis

Specimens were cut and polished in order to measure the transverse crack densities along the length of the specimen. The final, saturated, crack densities for HN-C-STD and HN-C-ENH composites were found to be ~ 2.1 and ~ 4.6 cracks/mm, respectively. The significantly smaller crack density and the significantly wider hysteresis loop-width for the HN-C-STD composites infer that the interfacial shear (sliding) stress, τ , for these composites were significantly lower than for the HN-C-ENH composites. τ can be estimated from hysteresis loop widths, $\delta\epsilon_{\max}$, from the relationship [13]:

$$\tau = (\sigma_p^2 / 2\delta\epsilon_{\max}) [b_2(1-a_1f)^2(R_f\rho_c) / \{4f^2E_m\}] \quad (3)$$

where σ_p is the peak hysteresis loop stress, R_f is the fiber radius, ρ_c is the matrix crack density, E_m is the matrix modulus, and a_1 and b_2 are constants based on the elastic properties of the constituents [16]. From equation (3), for the HN-C-STD composite τ was estimated to be ~ 31 MPa whereas for the HN-C-ENH composite τ was estimated to be ~ 350 MPa. These values may be overestimates due to the stiffening of the hysteresis loop at low stresses and the probable overlap of sliding lengths around cracks; however, the average pullout lengths of fibers on the fracture surfaces differed between the two composites by over an order of magnitude (> 1 mm for the HN-C-STD composite and ~ 50 μm for the HN-C-ENH composite) confirming at least the qualitative difference in the interfacial shear stresses for the composite systems. This is important because the amount of crack opening is strongly dependent on the interfacial sliding stress between the fiber and the matrix, as will be discussed below.

DISCUSSION

The relationship between non-linearity in the stress-strain curve associated with transverse matrix cracking, acoustic emission, and speed of sound measurements were in accord with previous studies. However, in this study it was demonstrated that the speed of the extensional sound wave was sensitive to the stiffening of the composite upon unloading due to crack closure. Therefore, the speed of sound can be used to monitor changes in a materials elastic properties that are dependent on stress without further damage.

The major finding of this study was the differences in attenuation of transmitted sound waves across a specimen at different stress states. For the lower τ material, HN-C-STD, the attenuation of the flexural sound waves produced by lead breaks was sensitive to the applied static stress for specimens which had been pre-loaded to at least 207 MPa. In other words, for sound waves created at zero stress after loading to 207 MPa, no significant additional attenuation occurred in comparison to undamaged material. However, for the same damaged material when loaded to 69 MPa or greater, a significant loss in signal was observed across the specimen. For the higher τ material, HN-C-ENH, no significant additional attenuation was observed when compared to undamaged material, even for specimens tested to 330 MPa. For both systems, many matrix cracks would have been present at 207 MPa. In fact, based on AE activity and the measured crack densities of failed specimens, the HN-C-ENH composites would have twice as many cracks as the HN-C-STD composites. Therefore, it is not just the presence of matrix cracks that causes the significant attenuation. The degree of crack opening must also play a major role in the attenuation of the acoustic signal. Assuming only frictional forces at the interface, the crack opening displacement, u , can be estimated by equation (4) [17].

$$u = 2\sigma^2 R / \{4 \tau f^2 E_f [1 + f E_f / (1-f) E_m]\} \quad (4)$$

Based on the τ values derived from the above analysis of the hysteresis loops (equation 3), the crack opening for HN-C-STD would be an order of magnitude greater than the crack opening for HN-C-ENH at a given stress. Since significant damping occurs between 138 and 207 MPa for the HN-C-STD material and no real increase in damping occurred for the HN-C-ENH material, it can be concluded that a certain combination of matrix crack density and crack opening displacement, i.e. low τ , is required for significant increases in attenuation as a function of increasing stress. This may be of special importance for applications where one wants to tailor the damping properties for a given application or increase the damping capacity of a material with increasing stress.

CONCLUSIONS

1. The speed of sound of the extensional wave was shown to be a reliable measure of the loss in stiffness due to damage accumulation as well as an increase in stiffness at zero stress after unloading due to crack closure.
2. The AE equipment was used to measure the attenuation of the transmitted sound waves created by lead-breaks and showed that a significant loss in signal was observed for composites with a low interfacial shear stress when the specimens were subject to an applied stress. However, at zero stress after unloading from a high pre-load stress, those same specimens showed no additional attenuation compared to undamaged material because of crack closure. In other words, the amount of attenuation for the low τ composite was dependent on the amount of damage and the applied stress at which attenuation measurements were made. For the high τ composite, no real change in attenuation was observed with increasing stress or damage compared to undamaged material.
3. Once the stress and/or damage-dependent acoustic properties are understood and quantified for a given composite system, the AE behavior can be used to monitor the stiffness of a material and the degree of damage accumulation in a component over a loading cycle. Conversely, if a certain stress-dependent acoustic damping property is required for an application, the microstructure of these types of composites can possibly be tailored to the desired acoustic properties required.

REFERENCES

1. Evans, A.G. and Zok, F.W., The physics and mechanics of fibre-reinforced brittle matrix composites. *J. Mat. Sci.*, 1994; 29; 3857-3896.
2. Brewer, D. HSR/EPM combustor materials development program. *Mater. Sci. Eng.*, 1999; A261; 284-291.
3. Kim, R.Y. and Pagano, N.J., Crack initiation in unidirectional brittle matrix composites. *J. Amer. Ceram. Soc.* 1991; 74; 1082-1090.
4. Luo, Y-J, Chang, S-C, and Daniel, I.M., Acoustic Emission Study of Failure Mechanisms in Ceramic Matrix Composites under Longitudinal Tensile Loading, *J. of Comp. Mater.* 1995; 29; 1946-1961.
5. Jenkins, M.G., Piccola, J.P., and Lara-Curzio, E., Onset of Cumulative damage and the Effects of Test Parameters on the Tensile Behavior of Continuous Fiber-Reinforced Ceramic Composites (CFCC), in *Fracture Mechanics of Ceramics*, Vol. 12., Ed. R.C. Bradt, D.P.H. Hasselman, D. Munz, M. Sakai, and V.Y. Shevchenko, Plenum Publishing Corp., USA, 1996, pp. 267-282.

6. Surgeon, M., Vanswijghoven, E., Wevers, M., and Van Der Biest, O., Acoustic emission during tensile testing of SiC-fibre-reinforced BMAS glass-ceramic composites. *Composites Part A*; 1997; 28A; 473-480.
7. Morscher, G.N., Modal acoustic emission of damage accumulation in a woven SiC/SiC composite. *Comp. Sci. Tech.* 1999; 59; 419-426.
8. Morscher, G.N., "Use of Modal Acoustic Emission for Source Identification in Woven SiC/SiC Composites," in Review of Progress in Quantitative Nondestructive Evaluation, Vol. 19, , D.O. Thompson and D.E. Chimenti, Eds., Kluwer Academic/Plenum Publishers, 2000; pp.383-390.
9. Gorman, M.R. Plate wave acoustic emission. *J. Acoust. Soc. Am.* 1990; 1; 358-364.
10. Gorman, M.R. and Ziola, S.M. Plate waves produced by transverse matrix cracking. *Ultrasonics.* 1991; 29; 245-251.
11. Tiwari, A. Real time acousto ultrasonic NDE technique for monitoring damage in ceramic composites under dynamic loads. NASA CR-198374, August 1995.
12. Kaiser, J., Erkenntnisse und Folgerungen aus der Messung von Gerauschen bei Zugbeanspruchung von Metallischen Werkstoffen. *Arch. Eisenhutten Wes.*, 1953; 24; 43-45.
13. Domergue, J.M., Heredia, F.E., and A.G. Evans, Hysteresis loops and the inelastic deformation of 0/90 ceramic matrix composites. *J. Am. Ceram. Soc.* 1996; 79; 161-170.
14. Steen, M. and Valles, J-L. Unloading-reloading sequences and the analysis of mechanical test results for continuous fiber ceramic composites. In: Thermal and Mechanical Test Methods and Behavior of Continuous-Fiber Ceramic Composites, ASTM STP 1309, Jenkins et al. (Eds.), ASTM, West Conshohocken, PA. 1997; pp. 49-65.
15. Domergue, J.M., Vagaggini, E., and Evans, A.G. Relationships between hysteresis measurements and the constituent properties of ceramic matrix composites: II, experimental studies on unidirectional materials. *J. Am. Ceram. Soc.* 1995; 78; 2721-2731.
16. Hutchnison, J.W. and Jensen, H.M. Models of fiber debonding and pullout in brittle composites with friction. *Mechanics of Materials*; 1990; 9; 139-163.
17. Marshall, D.B., Cox, B.N., and Evans, A.G. The mechanics of matrix cracking in brittle-matrix fiber composites. *Acta metal*; 1985; Vol. 33; No. 11; 2013-2021

Table I: Constituents of Hi-NicalonTM * Composites Tested

Composite	Volume fraction of fiber	Matrix	Porosity, %	Elastic Modulus, GPa
HN-C-CVI	0.29	Standard CVI SiC	30.0	177
HN-C-ENH	0.31	Enhanced CVI SiC	31.5	180

* Hi-NicalonTM Fiber: diameter = 13 μm ; $E_f = 270$ GPa

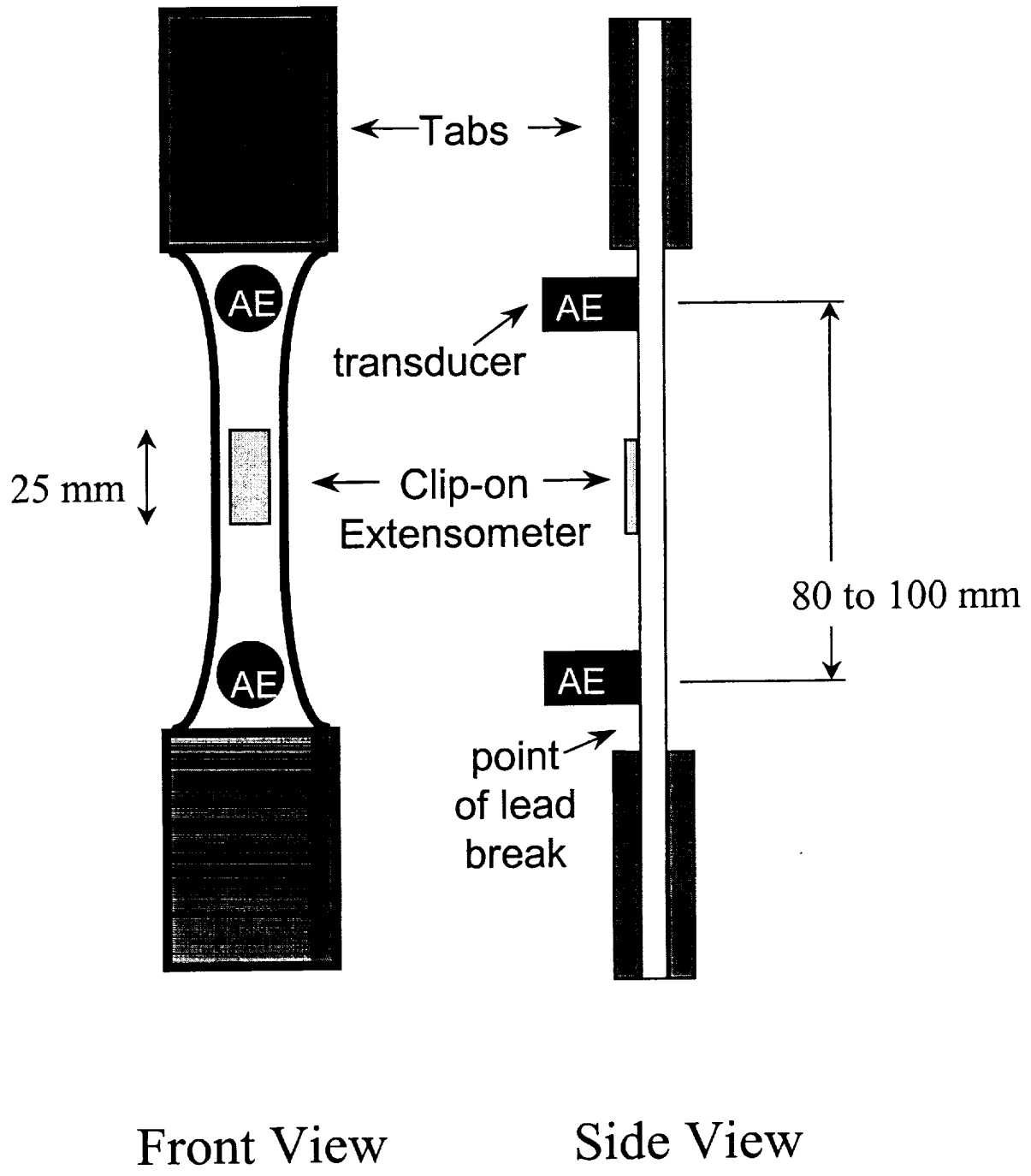


Figure 1: Schematic representation of tensile test specimen and sensor alignment.

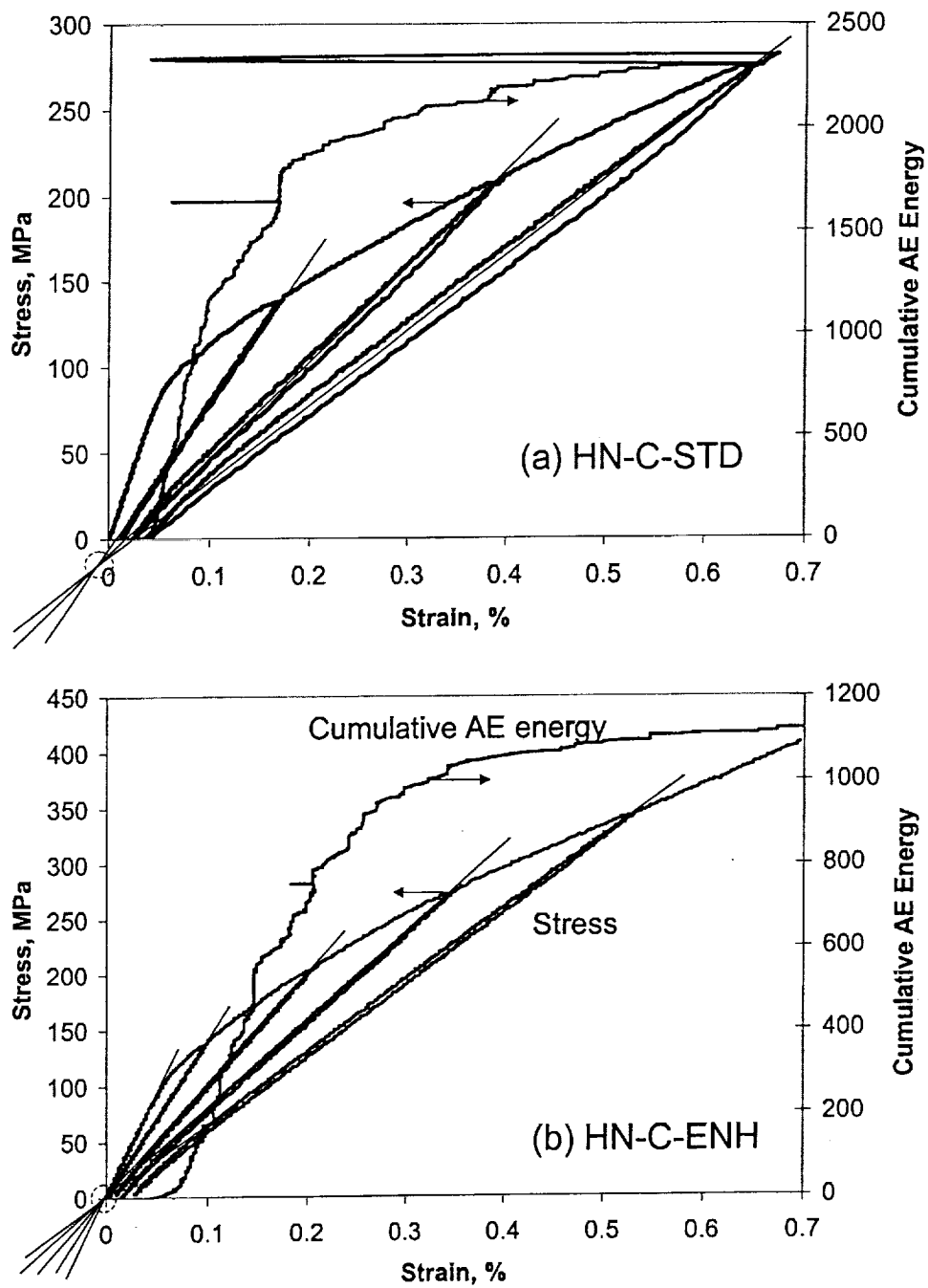


Figure 2: Typical tensile hysteresis stress-strain curves and AE energy cumulated during the tensile test from the events that occurred in the gage section for a (a) HN-C-STD and (b) HN-C-ENH composite specimens. The lines through the hysteresis loops are for the graphical construct, after Steen [14].

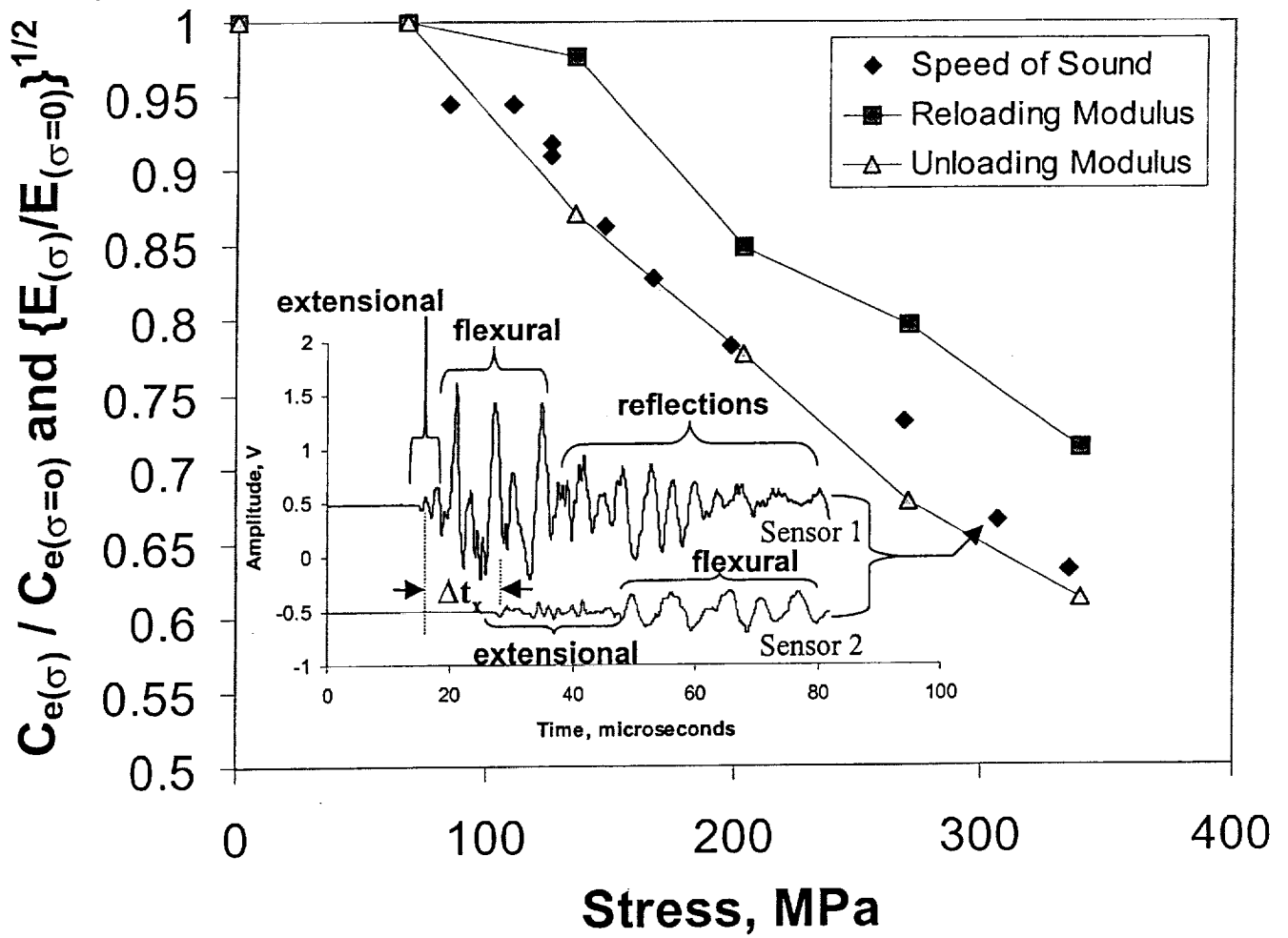
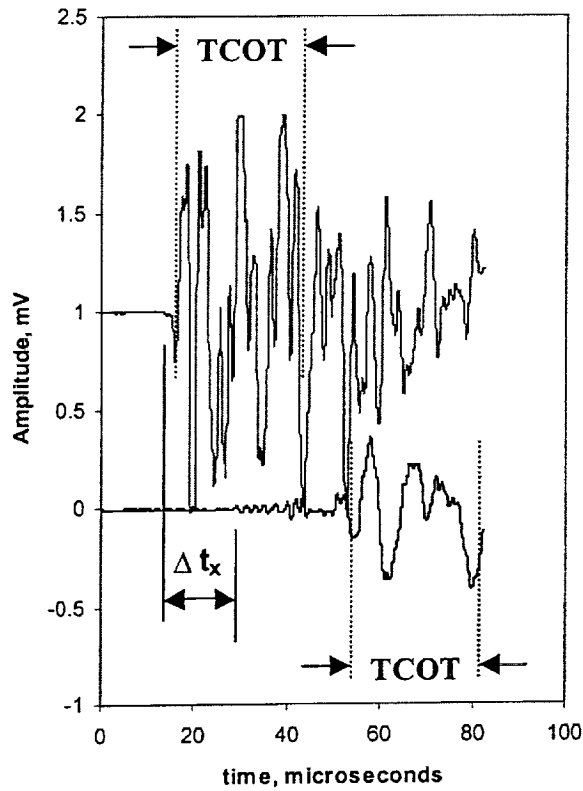
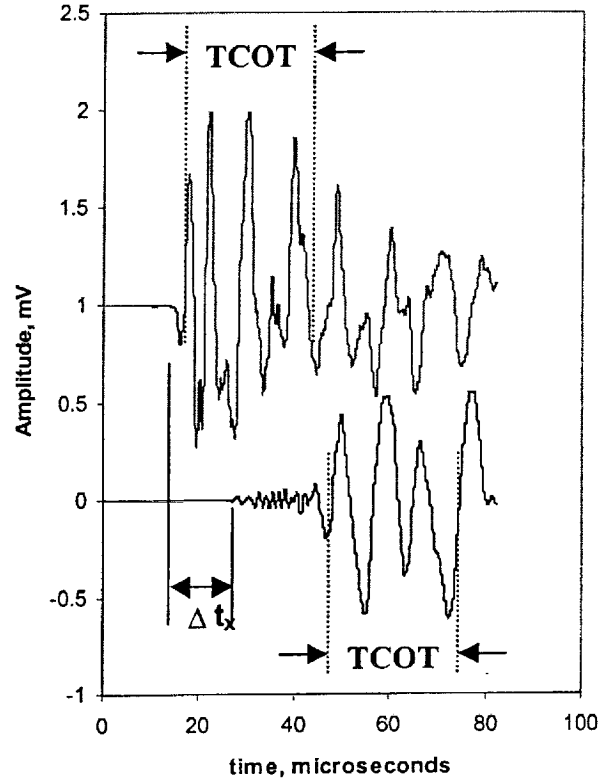


Figure 3: Normalized velocity of sound and elastic moduli for initial unloading and reloading portions of tensile hysteresis loops for a HN-C-ENH composite. Also shown are the two acoustic waveforms for one of the events used to measure speed of sound and the modal components of each waveform. For clarity, the waveforms are displaced ± 0.5 volts for the waveform on sensor 1 and sensor 2, respectively.

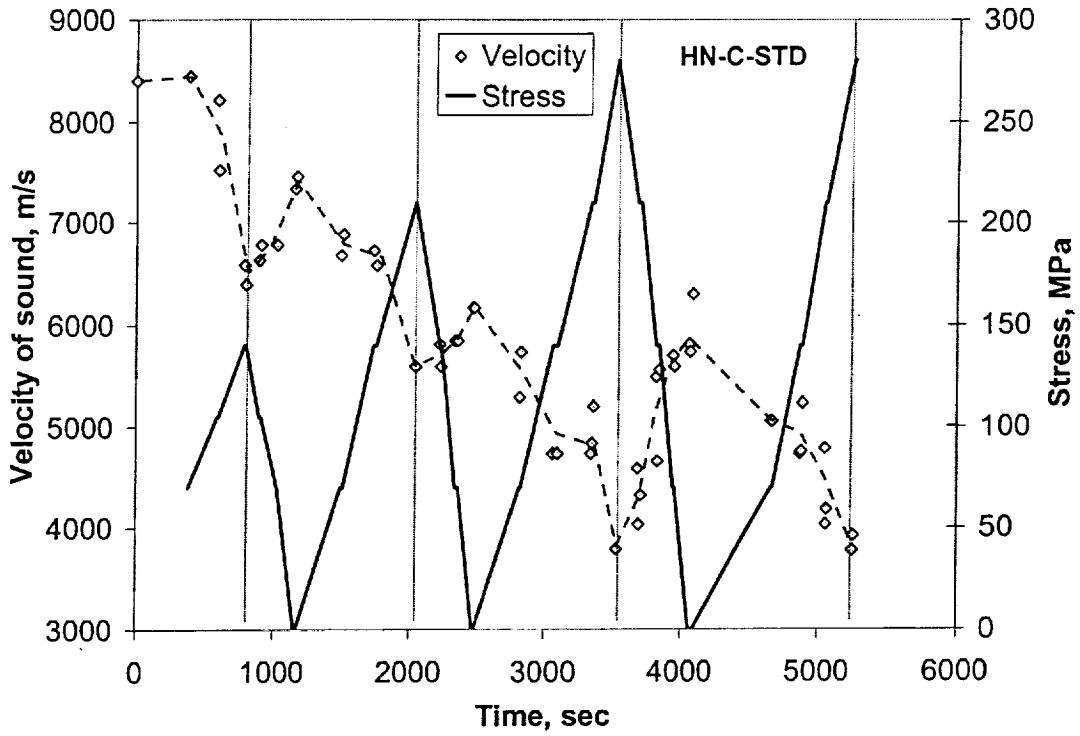


(a)

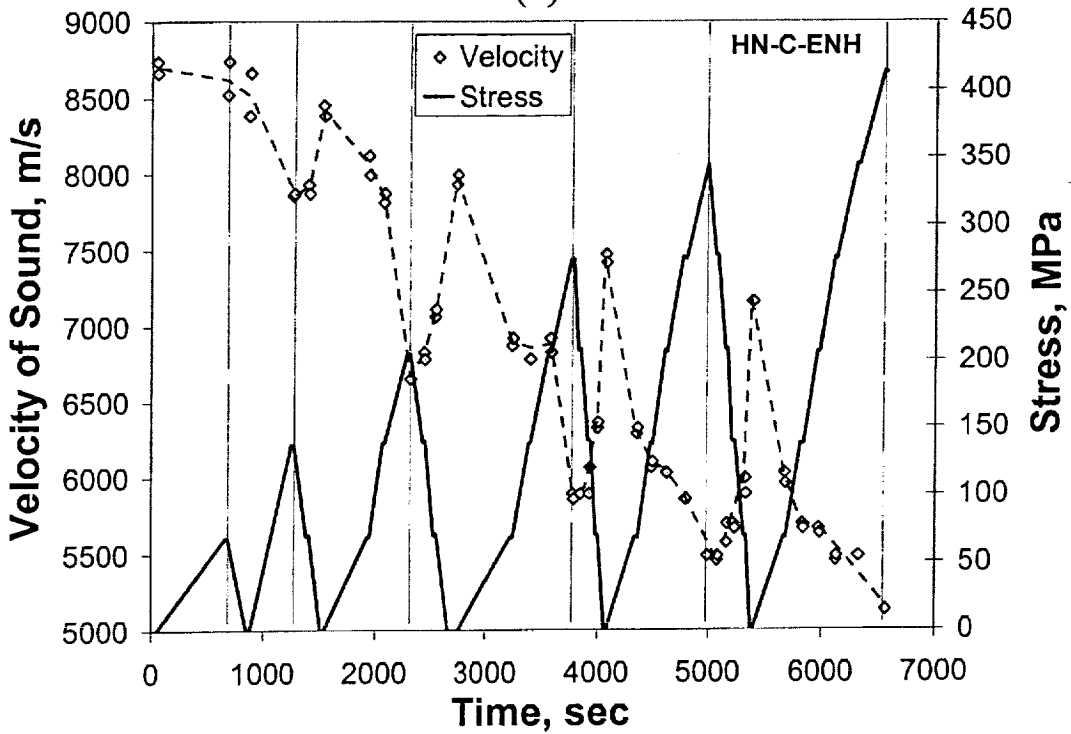


(b)

Figure 4: Waveforms from lead breaks captured on the sensor closest to the lead break (top waveform) and furthest from the lead break (bottom waveform) for a peak hysteresis stress of 210 MPa at (a) the peak stress and (b) zero stress after unloading for HN-C-STD. TCOT refers to the time frame over which the energy was determined in order to measure attenuation.

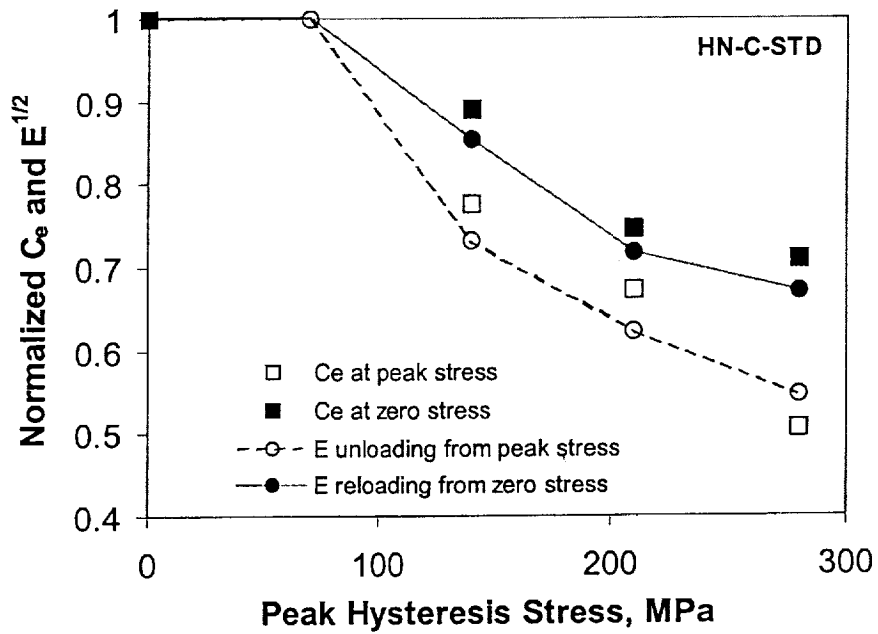


(a)

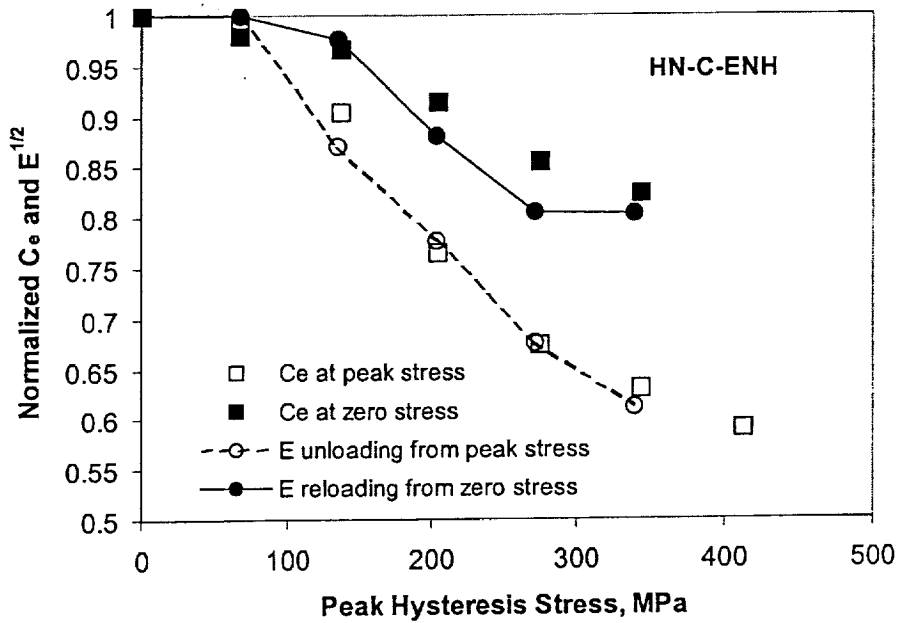


(b)

Figure 5: Speed of sound of the extensional wave and applied stress for (a) HN-C-STD and (b) HN-C-ENH composites.

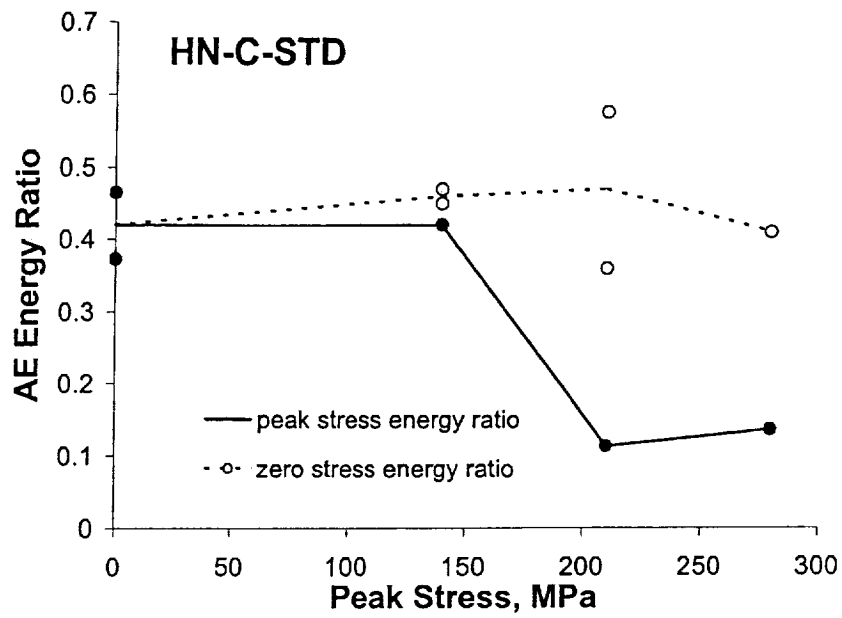


(a)

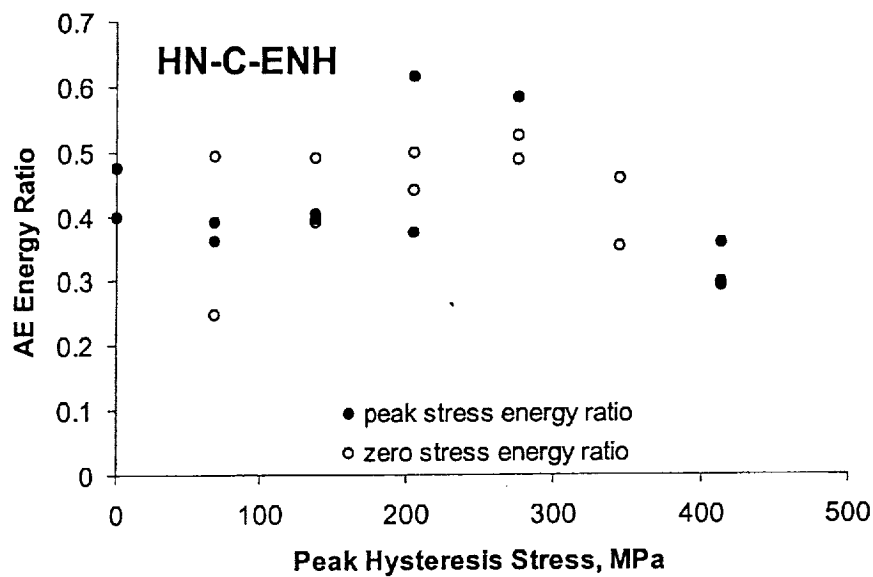


(b)

Figure 6: The normalized speed of sound and square root of the elastic modulus for different peak stress hysteresis loops in (a) HN-C-STD and (b) HN-C-ENH composites.



(a)



(b)

Figure 7: Ratio of AE energy, i.e. TCOT energy of far sensor divided by the TCOT energy of near sensor, for lead breaks made at the peak stress and at zero stress after a certain peak stress for (a) HN-C-STD and (b) HN-C-ENH composites.

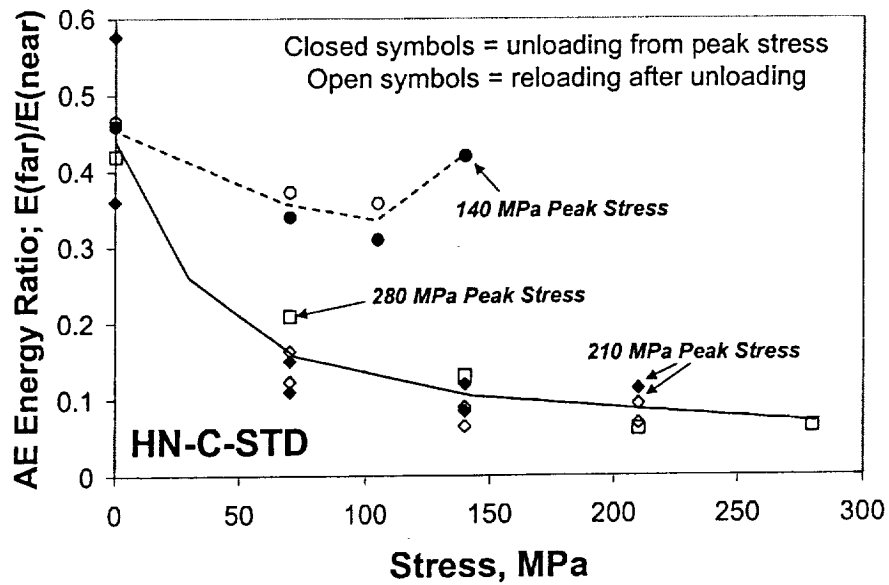


Figure 8: The ratio of AE energy, i.e., TCOT energy of far sensor divided by TCOT energy of near sensor for lead breaks made at peak, intermediate, and zero stresses for individual hysteresis loops of a HN-C-STD composite